

Dark matter admixed neutron stars with a realistic nuclear equation of state from chiral nuclear interactions

Domenico Scordino^a, Ignazio Bombaci^{a,b},

^a*Dipartimento di Fisica “E. Fermi”, Università di Pisa, Largo B. Pontecorvo 3, I-56127 Pisa, Italy*

^b*INFN, Sezione di Pisa, Largo B. Pontecorvo 3, I-56127 Pisa, Italy*

(Dated: May 30, 2024)

We study the effects of dark matter on the structural properties of neutron stars. In particular we investigate how the presence of a dark matter component influences the mass-radius relation, the value of the maximum mass of a neutron star and others stellar properties. To model ordinary matter we use a state-of-the-art equation of state of β -stable nuclear matter obtained using the Brueckner-Hartree-Fock quantum many-body approach starting from two-body and three-body nuclear interactions derived from chiral effective field theory. The dark matter component of the star is modeled as a non-self-annihilating system of spin 1/2 fermions and its equation of state as an ideal relativistic Fermi gas. The equilibrium configurations of these dark matter admixed neutron stars (DANS) are calculated by solving a generalization of the Tolman-Oppenheimer-Volkoff equations to the case where the system consists of two perfect fluids interacting solely through gravity. We find that, depending on the dark matter particle mass m_χ , one can have somehow opposite effects on the stellar properties. In the case $m_\chi = 1 \text{ GeV}$, the stellar gravitational maximum mass M_{max} decreases, whereas in the case $m_\chi = 0.1 \text{ GeV}$, M_{max} increases with respect to the maximum mass of ordinary neutron stars. We also show that the presence of dark matter has indirect sizeable effect on the proton fraction in the ordinary matter fluid and, in the case $m_\chi = 1 \text{ GeV}$, results in a decrease of the threshold gravitational mass M_{tot}^{durca} for having direct URCA processes and fast stellar cooling. Finally we study the stability of dark matter admixed neutron stars with respect to radial perturbations.

I. INTRODUCTION

In spite of its many successes, Einstein’s theory of general relativity provides predictions that are at variance with astrophysical observational data on the kinematics of self-gravitating systems as galaxies and clusters of galaxies [1, 2]. In order to reproduce these data using general relativity requires the introduction of a new type of matter, known as dark matter (DM), that is not directly observable except through its gravitational effects on ordinary matter. Cosmological data, currently explained by the Λ -cold dark matter (Λ CDM) model [3], indicate that DM should be responsible for about 23% percent of the total energy density of the Universe while ordinary matter (OM) contributes only 4%. The remaining portion is due to dark energy responsible for the accelerated expansion of the Universe [4, 5].

The main feature of DM is that its cross section for electromagnetic processes must be extremely small or zero. As a result, DM cannot lose energy by emitting electromagnetic radiation, as in the case of ordinary matter, and thus DM does not collapse at the center of galaxies. In fact, the rotation curve profiles of disc galaxies (i.e. the plot of the orbital speeds of visible stars or gas in the galaxy versus their radial distance from the galaxy’s centre) are in agreement with the presence of an extended and diffuse halo of DM (see [6–8]).

None of the particles of the standard model meet the requirements for explaining the numerous astrophysical observations and cosmological data that require the existence of dark matter. Thus candidate particles to consti-

tute dark matter most often emerge from extensions of the standard model. A much-studied class of such particles are WIMPs (weakly interacting massive particles), and many active experiments are attempting to reveal their existence. No such experiments, however, have so far obtained convincing results on the existence of DM particles even though very stringent constraints on the interaction cross section of dark matter with ordinary matter have been produced (see e.g. [9]). If such a cross section is nonzero (although very small), it is conceivable that DM could be captured by stars or compact stellar objects, especially in environments such as the Galactic center, in a sufficient amount to produce observable effects.

Due to the very high densities ($10^{14} - 10^{15} \text{ g/cm}^3$) in their cores, the extreme surface gravity ($g \sim 10^{12} \text{ m/s}^2$) and their ages (up to 10^{10} yr), neutron stars are very good candidates where dark matter can be captured and can accumulate in sufficient amounts to influence their structural and evolutionary properties. Neutron stars can thus be used as natural detectors to identify DM and possibly unveil its nature [10–23].

In this paper we study the effects of the presence of DM on the structure and stability of neutron stars. In particular, we investigate, in a very detailed and systematic way, how the properties of these Dark matter Admixed Neutron Stars (DANS) are modified with respect to those of ordinary neutron stars in terms of the peculiarities and the fraction of DM present in the star.

The comparison of the results for the properties of DANS obtained in this work with some observational

properties of neutron stars, such as the values of their gravitational mass (especially those of "massive" stars with $M \sim 2M_\odot$ that place stringent constraints on the value of the Oppenheimer-Volkoff mass limit) or the combined mass and radius measurements (obtained from NASA's NICER X-ray observatory) allowed us to derive constraints on the mass of the dark matter particles and the fraction of dark matter present in the star.

This work is organized as follows. In Section II, we introduce the two-fluids Tolman-Oppenheimer-Volkoff (TOV) stellar structure equations. In Section III, we discuss the equation of state for OM and for DM used in the present work. In Section IV we present results obtained by solving the two-fluids TOV equation and discuss the properties of DANS. In Section V we use observational data for properties of neutron stars to determine an upper limit to the dark matter particle mass. In Section VI, we study the stability of DANS equilibrium configurations with respect to small radial perturbations. Finally, in Section VII we give a brief summary of our work.

II. STRUCTURE EQUATIONS FOR DANS

Since the non-gravitational interaction between dark matter and ordinary matter is extremely small (e.g. [9, 24]), it is possible to split the total energy-momentum tensor as the sum of the energy-momentum tensor of each of the two fluids (OM and DM) and to have covariant conservation for both of them. Accordingly, the equation of state of OM is independent on the state variables of DM and vice versa. In addition, it is assumed that each of the two fluids be a perfect fluid. Based on these assumptions, and further assuming a spherically symmetric and stationary distribution of OM and DM, the stellar structure equations in general relativity for DANS take the following form (see e.g. [21]), which generalizes the TOV equations to the case of two fluids interacting exclusively through gravity:

$$\frac{dP_j}{dr} = -G \frac{m_{tot}(r) \varepsilon_j(r)}{c^2 r^2} \left(1 + \frac{P_j(r)}{\varepsilon_j(r)} \right) \times \left(1 + \frac{4\pi r^3 P_{tot}^3(r)}{c^2 m_{tot}(r)} \right) \left(1 - \frac{2G m_{tot}(r)}{c^2 r} \right)^{-1} \quad (1)$$

and

$$\frac{dm_j(r)}{dr} = \frac{4\pi}{c^2} r^2 \varepsilon_j(r), \quad (2)$$

where G is the gravitational constant, P_j and ε_j (with $j = \text{OM, DM}$) are the pressure and energy density for the OM and DM fluid, $m_j(r)$ is the gravitational mass enclosed within a sphere of radial coordinate r (surface area $4\pi r^2$) for each of the two fluids, $m_{tot}(r) = m_{OM}(r) + m_{DM}(r)$ is the total gravitational mass enclosed within a sphere of radial coordinate r and $P_{tot}(r) = P_{OM}(r) + P_{DM}(r)$ the total pressure.

A. Numerical integration

To solve the stellar structure equations (1) and (2) we need to specify the equation of state for the two fluids (see next section) and the appropriate boundary conditions at the center ($r = 0$) and at the surface ($r = R_j$, $j = \text{OM, DM}$) of the matter distribution for each fluid [21]:

$$m_j(0) = 0 \quad \varepsilon_j(0) = \varepsilon_{c,j}$$

We define the radius R_j of the distribution of fluid j by the following condition

$$P_j(R_j) = P_j^{surf}$$

where P_j^{surf} is a fixed value for the surface pressure of fluid j . For dark matter we use $P_{DM}^{surf} = 0$ while for ordinary matter we chose $P_{OM}^{surf} = P_{OM}(\rho^*)$, where $\rho^* = 7.86 \text{ g/cm}^3$ is the mass density of solid ^{56}Fe . For $r > R_j$ we define $P_j(r) = 0$. The total radius of the star is

$$R = \max\{R_{OM}, R_{DM}\} \quad (3)$$

Integrating Eq.(2) we get the total gravitational mass M_j for each of the two fluids ($j = \text{OM, DM}$)

$$M_j \equiv m_j(R_j) = \frac{4\pi}{c^2} \int_0^{R_j} r^2 \varepsilon_j(r) dr \quad (4)$$

and the total gravitational mass of the DANS is

$$M_{tot} = M_{OM} + M_{DM}. \quad (5)$$

III. EQUATION OF STATE

A. The equation of state of ordinary matter

In this work we model the OM fluid of a DANS as a uniform electric-charge-neutral fluid of neutrons, protons, electrons, and muons. Recently a new microscopic EOS for this system has been obtained in Ref. [25] (hereafter the BL EOS) for the zero temperature case, using the Brueckner-Hartree-Fock (BHF) quantum many-body approach (see [25] and references therein) starting from modern two-body and three-body nuclear interactions derived within chiral effective field theory (ChEFT) (e.g. [26, 27]). These chiral nuclear interactions reproduce with high accuracy the nucleon-nucleon (NN) scattering data and the experimental binding energies of light ($A = 3, 4$) atomic nuclei [28]).

The BL EOS reproduces the empirical saturation point (i.e. saturation density $n_0 = 0.16 \pm 0.01 \text{ fm}^{-3}$, and energy per nucleon $E/A|_{n_0} = -16.0 \pm 1.0 \text{ MeV}$) of symmetric nuclear matter, and other empirical properties (symmetry energy E_{sym} and its slope parameter L , incompressibility) of nuclear matter at the saturation density n_0 (see

Tab. 2 in [25]). In particular the calculated $E_{sym}(n_0)$ and L for this EOS fulfill the bounds imposed by the unitary Fermi gas limit [29, 30]. As has been shown in ref. [29] several EOS models currently used in neutron star structure calculations, in supernova explosions and binary neutron star mergers simulations violate the unitary Fermi gas bounds.

Further the BL EOS is consistent (see figure 2 in [25]) with the measured elliptic flow of matter in heavy-ion collisions experiments [31].

At supranuclear densities ($n > n_0$) the BL EOS model predicts a symmetry energy $E_{sym}(n)$ which is in very good agreement with the empirical constraints derived in [32] using the excitation energies of isobaric analog states in nuclei and with additional constraints from neutron skin thickness of heavy nuclei [33]. As is well known, the symmetry energy $E_{sym}(n)$, and particularly its density dependence is a crucial ingredient to determine the proton fraction in β -stable nuclear matter [34–37] and ultimately it has an impact on the value of stellar radius and on the thickness of the crust [38, 39] and on the possibility of having direct URCA processes [40] (see Section IV B) and thus rapid cooling of neutron stars [41].

When computing static ordinary neutron star configurations the BL EOS (for the β -stable case) gives [25] a maximum mass $M_{\max} = 2.08 M_{\odot}$, with a corresponding central density $\rho_c = 2.74 \times 10^{15} \text{ g/cm}^3$ and radius $R(M_{\max}) = 10.26 \text{ km}$ and a quadrupolar tidal polarizability coefficient $\Lambda_{1.4} = 385$ (for the $1.4 M_{\odot}$ neutron star [42]) compatible with the constraints derived from GW170817 [43].

Recently, the BL EOS has been extended [44] to finite temperature and to arbitrary proton fractions. This finite-temperature EOS model has been applied to numerical simulations of binary neutron star mergers [45–47].

Finally, to model the (ordinary) neutron star crust (i.e. for nucleonic density $\leq 0.08 \text{ fm}^{-3}$) we have used the Baym–Pethick–Sutherland [48] and the Negele–Vautherin [49] EOS.

B. The equation of state of dark matter

In the present work we consider non-self-annihilating fermionic DM. This so called fermionic asymmetric dark matter (ADM) [50, 51] carry a conserved charge which is analogous to the baryon number in the case of ordinary matter. We describe the ADM fluid as a non-interacting (ideal) gas of fermions with mass m_{χ} and spin 1/2. The corresponding EOS is well known (see e.g. [52]) and is given by the following expressions

$$\begin{aligned}\varepsilon(x) &= \alpha(m_{\chi}, \nu)\chi(x) \\ p(x) &= \alpha(m_{\chi}, \nu)\phi(x) \\ n(x) &= n_0(m_{\chi}, \nu)x^3\end{aligned}$$

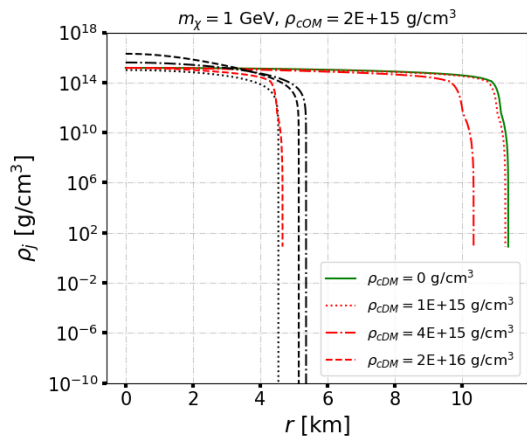


FIG. 1. Mass-density profiles of ordinary matter (red) and dark matter (black) to the two-fluids TOV equation for $m_{\chi} = 1 \text{ GeV}$, $\rho_{cOM} = 2 \times 10^{15} \text{ g/cm}^3$ and different values of the dark matter central densities ρ_{cDM} . Each line-style correspond to a different choice of ρ_{cDM} : ($\rho_{cOM}, 0$) (green continuous line), ($\rho_{cOM}, 10^{15} \text{ g/cm}^3$) (dotted lines), ($\rho_{cOM}, 4 \times 10^{15} \text{ g/cm}^3$) (dash-dot lines), ($\rho_{cOM}, 2 \times 10^{16} \text{ g/cm}^3$) (dashed lines).

ρ_{cDM} [g/cm ³]	M_{OM} [M _⊙]	M_{DM} [M _⊙]	f_{χ} [%]	R_{OM} [km]	R_{DM} [km]
0	1.895	0	0	11.375	0
10^{15}	1.740	0.050	2.78	11.287	5.542
4×10^{15}	1.059	0.240	18.44	10.345	5.365
2×10^{16}	0.095	0.453	82.62	4.664	5.148

TABLE I. Values for the gravitational mass of ordinary matter and dark matter and total fraction of dark matter obtained for $m_{\chi} = 1 \text{ GeV}$, $\rho_{cOM} = 2 \times 10^{15} \text{ g/cm}^3$ and different values of the dark matter central mass-density.

where $x \equiv \hbar k_F / (m_{\chi} c)$ is the adimensional Fermi momentum, the degeneracy factor $\nu = 2$ for spin 1/2 particles and

$$\begin{aligned}\alpha(m_{\chi}, \nu) &= \nu \frac{\hbar c}{16\pi^2} \left(\frac{m_{\chi} c^2}{\hbar c} \right)^4 \\ n_0(m_{\chi}, \nu) &= \nu \frac{(m_{\chi} c^2)^3}{6\pi^2 (\hbar c)^3} \\ \chi(x) &= x(1+x^2)^{1/2}(1+2x^2) - \ln[x + (1+x^2)^{1/2}] \\ \phi(x) &= x(1+x^2)^{1/2} \left(\frac{2}{3}x^2 - 1 \right) + \ln[x + (1+x^2)^{1/2}]\end{aligned}$$

IV. DANS PROPERTIES

For a fixed values of the dark matter particle mass m_{χ} , a solution the two-fluid TOV equations (1) and (2) is uniquely identified once we fix the central mass densities (central energy densities) ρ_{cOM} and ρ_{cDM} for the two fluids.

As an illustrative example, we display in Figure (1) the radial mass density profiles $\rho_{OM}(r)$ for OM (red curves)

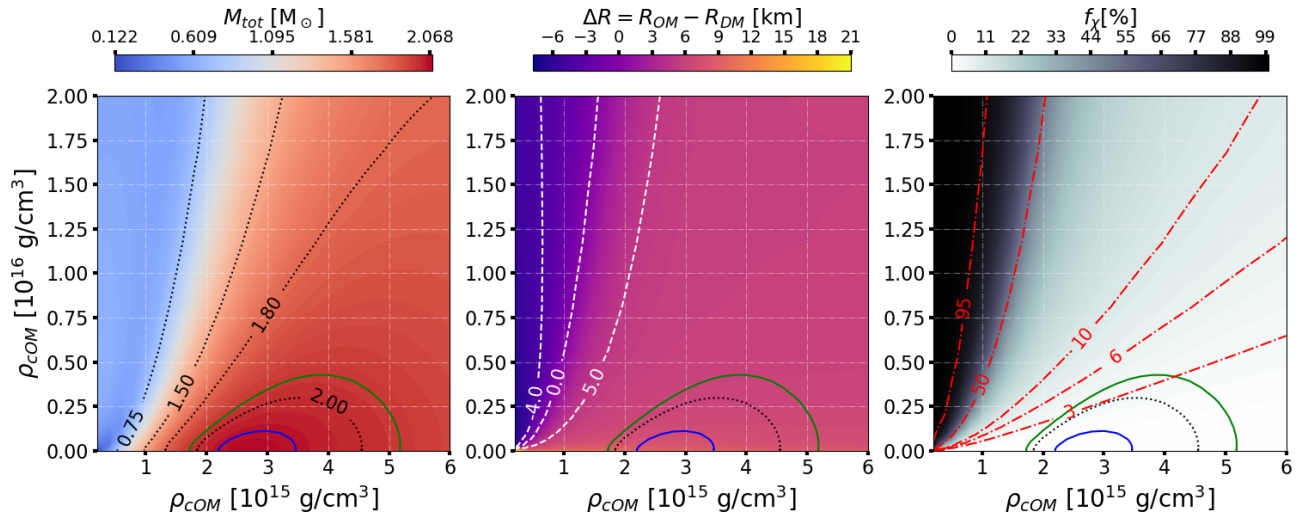


FIG. 2. Results for equilibrium configurations of DANS in the (ρ_{cOM}, ρ_{cDM}) plane for the case $m_\chi = 1$ GeV. The left panel shows the total gravitational mass of the star $M_{tot} = M_{tot}(\rho_{cOM}, \rho_{cDM})$ for different choices of the central mass densities. The central and right panel show the quantity $\Delta R = R_{OM} - R_{DM}$ and the stellar DM fraction in percent f_χ [%] respectively as function of the central mass densities. On each of the three panels we report the contour lines for M_{tot} (left), ΔR (central) and f_χ [%] (right). The green and blue lines in each panel delimit the region in the central mass density plane where the total gravitational mass M_{tot} is compatible with the measurement of the mass of the neutron star associated with the pulsar PSR J0348+0432 ($2.01 \pm 0.04 M_\odot$) [53].

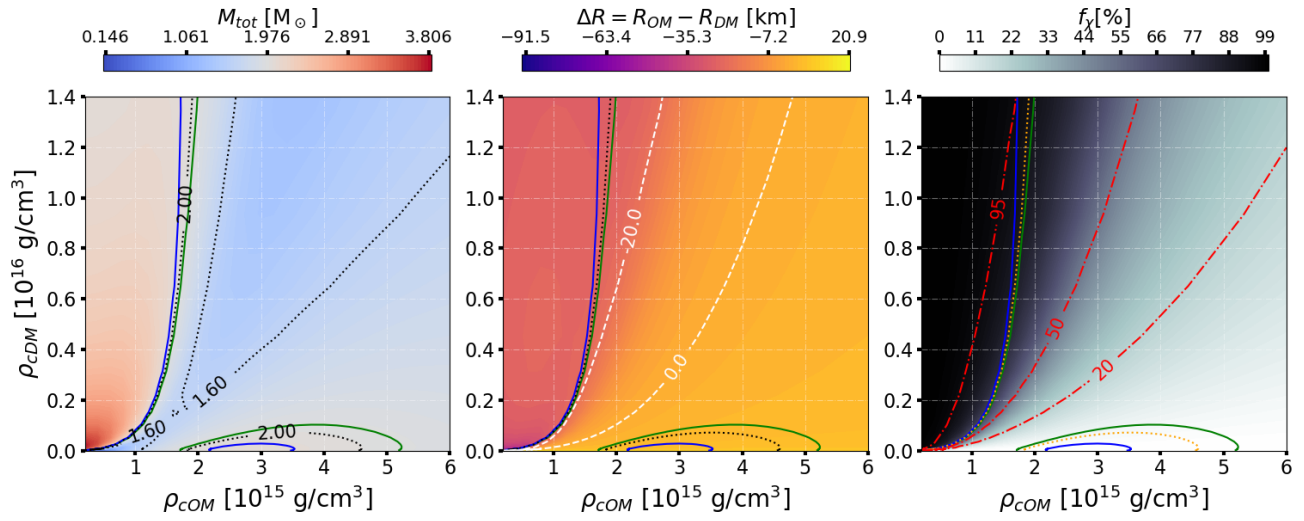


FIG. 3. Same as in Fig (2) but now for the the case $m_\chi = 0.4$ GeV.

and $\rho_{DM}(r)$ for DM (black curves) obtained for a fixed value $\rho_{cOM} = 2 \times 10^{15} \text{ g/cm}^3$ of the OM fluid central density and using different values ρ_{cDM} of the DM fluid central density. Each line-style in Figure (1) corresponds to the profiles obtained for a different value of ρ_{cDM} (see the figure caption for more details). As a baseline, we also plot in the same figure the mass density profile of an ordinary neutron star (green line). Taking the same stellar configurations considered in Figure (1), we report in Table (I) the total gravitational masses (eq.(4)) of the OM and DM stellar components, the corresponding radii R_{OM} and R_{DM} and the stellar DM fraction f_χ defined

as

$$f_\chi = \frac{M_{DM}}{M_{tot}}. \quad (6)$$

All the results reported in Figure (1) and in Table (I) are relative to the case $m_\chi = 1$ GeV. Coming back to Figure (1) we see that in the first two cases (dotted line and dash-dot lines), the radius of the dark matter distribution is smaller than the radius of the ordinary matter distribution ($R_{OM} \geq R_{DM}$) and thus we have a DANS with a dark matter core. In the third case reported in figure (1) (dashed lines) we have $R_{OM} < R_{DM}$ and thus

we have a DANS with a dark matter halo.

The results of our systematic calculations for hydrostatic equilibrium configurations of DANS in the (ρ_{cOM}, ρ_{cDM}) plane are reported in Fig (2) for the case $m_\chi = 1$ GeV. In particular, in the left panel we report, using a color scale, the total gravitational mass M_{tot} of the star. The black dotted lines represent the contour lines ($M_{tot} = \text{const}$), whereas the green and blue lines (reported in each of the three panels) are the contour lines which mark the region in the central mass densities plane where the calculated M_{tot} is compatible with the measured mass ($2.01 \pm 0.04 M_\odot$) [53] of the neutron star associated to the pulsar PSR J0348+0432. In the central panel of Fig (2), we report, using a color scale, the difference $\Delta R = R_{OM} - R_{DM}$ between the radii of the OM and DM fluid distributions. The white dashed line labeled by "0.0" represents the contour line $\Delta R = 0$ and thus marks the boundary between DANS with a DM core (on the right of the $\Delta R = 0$ line) and those with a DM halo (on the left of the $\Delta R = 0$ line). Finally, in the right panel of Fig (2) we plot the DM fraction (in percent) f_χ [%] and the contour lines for this quantity (red dash-dotted lines). The results in the right panel of Fig (2) ($m_\chi = 1$ GeV) clearly show that only DANS with a low DM fraction ($f_\chi < 4\%$) are compatible with the measured mass of the neutron star associated with PSR J0348+0432 and that these configurations are all characterized by the presence of a DM core (see middle panel). In Fig. (3) we show our results for DANS properties in the case $m_\chi = 0.4$ GeV. Now, in addition to the region of the (ρ_{cOM}, ρ_{cDM}) plane populated by DANS with a DM core and $f_\chi \lesssim 4.6\%$ and having $M_{tot} \sim 2 M_\odot$, there is a second region of the (ρ_{cOM}, ρ_{cDM}) plane populated by DANS with $M_{tot} \gtrsim 2 M_\odot$. All members of this second group of DANS have an extended DM halo and are almost completely formed by DM. In the $m_\chi = 0.4$ GeV case a large region of the (ρ_{cOM}, ρ_{cDM}) plane is populated by DANS with an extended DM halo and having a high DM fraction.

As a general trend, we have that for fixed values of the central mass densities of the two fluids, higher values of m_χ tend to favor the formation of a dark matter core, whereas lower values of m_χ tend to favor the formation of a dark matter halo.

A. Mass-radius relation for fixed f_χ

To investigate the effects of DM on observable properties of DANS, we consider stellar sequences with a fixed DM fraction f_χ . In other words, we solve the two-fluid structure equations by taking the central mass density of the OM fluid ρ_{cOM} and the DM fraction f_χ as independent variables.

In figure (4), for the case $m_\chi = 1$ GeV, we show the total gravitational mass of the star M_{tot} as a function of ρ_{cOM} (left panel) and M_{tot} as a function of the radius R_{OM}

of the OM fluid distribution (right panel). The surface of the OM fluid distribution is in fact the place where the electromagnetic radiation, that allows to determine R_{OM} , is generated. The light blue dash-dotted curve in both panels represents the ordinary neutron star sequence ($f_\chi = 0$). The other two curves represent DANS sequences with $f_\chi = 3\%$ (orange dash-dotted lines) and $f_\chi = 6\%$ (green dash-dotted lines). These two stellar sequences represent DANS having a DM core (see central and right panels in Fig (2)). The light green horizontal band represents the measured mass ($2.08 \pm 0.07 M_\odot$) [54] of the neutron star associated to the pulsar PSR J0740+6620, whereas the pink horizontal band represents the measured mass ($2.01 \pm 0.04 M_\odot$) [53] of the neutron star associated to the pulsar PSR J0348+0432. As we can see from the results reported in figure (4), the presence of DM with $m_\chi = 1$ GeV reduces the value of the maximum gravitational mass $M_{max} \equiv M_{tot,max}$ of the star with respect to the one for ordinary ($f_\chi = 0$) neutron stars. Considering DANS sequences with $f_\chi \gtrsim 3\%$ the calculated maximum mass is no longer compatible with the present measured masses of "heavy" neutron stars with $M \sim 2 M_\odot$ [53, 54]. We also note that the $M_{tot}(\rho_{cOM})$ curve is shifted towards higher value of the ordinary matter central density ρ_{cOM} compared to the ordinary neutron stars case ($f_\chi = 0\%$) as f_χ increases. The presence of DM also affects the value of the OM radius R_{OM} (right panel) making the OM distribution more compact [18, 19]. For example, considering an ordinary neutron star with a gravitational mass $M = 1.4 M_\odot$, a DM fraction $f_\chi = 6\%$ reduces the stellar observable radius R_{OM} by ~ 0.6 km i.e by $\sim 5\%$. These changes in the stellar radius are within the bounds of uncertainty of present instruments, as NICER, for measuring neutron star radii. The orange region, in the right panel of Fig. (4), marks the NICER measurement for the mass and radius of the neutron star in PSR J0030+0451 [55] while the gray and blue regions represent the portion of the mass-radius plane compatible with the data obtained from the GW170817 event (at 90% *CL*) [56].

In Fig. (5) we report DANS sequences for DM particles having a mass $m_\chi = 0.1$ GeV and for fixed DM fraction. In this case we get stars with a DM halo. This leads to a growth of the total gravitational maximum mass M_{max} of the star as f_χ increases. Since the ordinary neutron star sequence, calculated with the BL EOS, is compatible with the present measured masses of "heavy" neutron stars, the agreement with the same observational data will clearly hold for DANS sequences in the $m_\chi = 0.1$ GeV case.

To investigate in details how the maximum mass M_{max} of DANS depends on the DM fraction f_χ and on the DM particle mass m_χ , we show in Fig. (6) our results for the function $M_{max}(m_\chi, f_\chi)$ calculated for a few constant values of m_χ (curves in different colors). The black heavy dot on top of each curve denotes the minimum of the function $M_{max}(f_\chi)$. We see that for $m_\chi \approx 0.188$ GeV the minimum of the orange curve is equal to $2 M_\odot$ (a

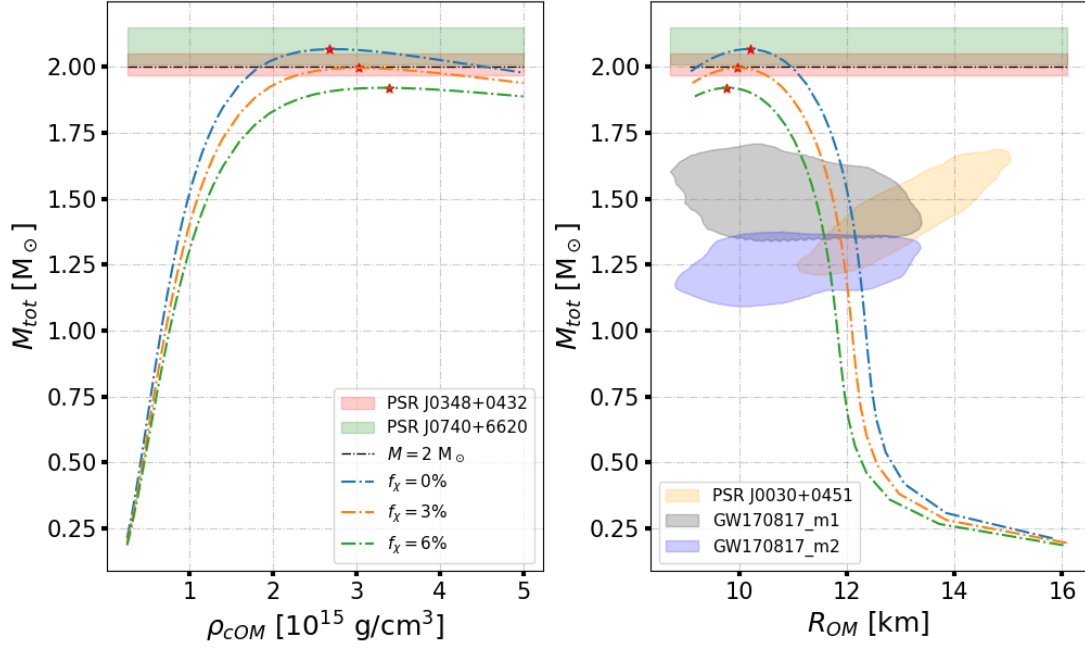


FIG. 4. Total gravitational mass of the star M_{tot} as a function of ρ_{COM} (left panel) and M_{tot} as a function of the radius R_{OM} of the OM fluid distribution (right panel) for different values of the DM fraction ($f_\chi = 0\%, 3\%, 6\%$) and in the case $m_\chi = 1$ GeV. The red star symbol on the top of each curve marks the maximum mass configuration. The light green and the pink horizontal bands represent respectively the measured mass of the neutron star associated to the pulsar PSR J0740+6620 [54] and to PSR J0348+0432 [53]. In the right panel, the orange region marks the NICER measurement for the mass and radius of the neutron star in PSR J0030+0451 [55] while the gray and blue regions represent the portion of the mass-radius plane compatible with the data obtained from the GW170817 event (at 90% CL) [56].

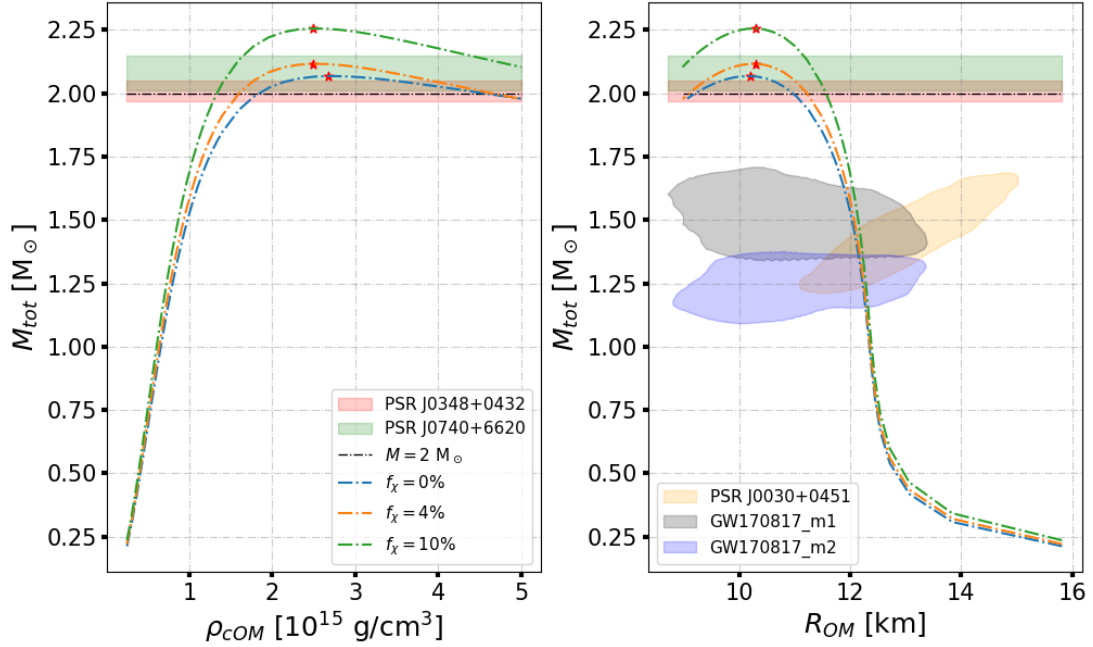


FIG. 5. Same as in Fig (4) but now for the the case $m_\chi = 0.1$ GeV and DM fraction $f_\chi = 0\%, 4\%, 10\%$.

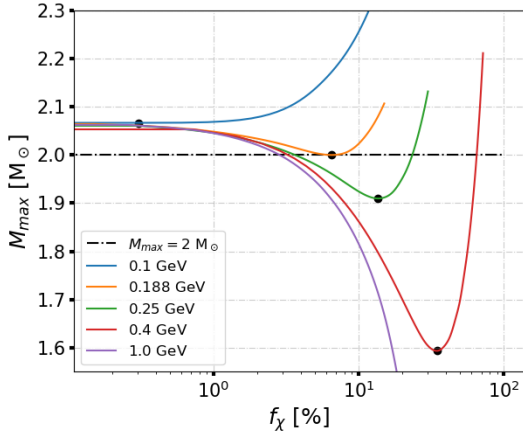


FIG. 6. Maximum mass for dark matter admixed neutron stars as a function of the dark matter fraction f_χ for fixed values of the dark matter particle mass m_χ . The black heavy dot on top of each curve denotes the minimum of each curve.

value we take as a reference for the measured masses of “heavy” neutron stars): this result means that for $m_\chi \leq 0.188$ GeV we obtain a value for M_{max} that is always compatible with measured neutron star masses for any value of f_χ .

Following [19, 57], for any fixed value of $m_\chi \geq 0.188$ GeV, we define a critical value of the DM fraction, and denote it with $f_\chi^{crit} = f_\chi^{crit}(m_\chi)$, as the solution of the equation $M_{max}(f_\chi, m_\chi) = 2 M_\odot$.

From figure (6) we see that for $0.188 \text{ GeV} \leq m_\chi \leq 0.4 \text{ GeV}$ we get two critical values for f_χ and we observe that the largest of the two roots tends to $f_\chi = 100\%$ as m_χ increases. For the considered values $m_\chi \geq 0.4 \text{ GeV}$ we get one critical value for f_χ .

The exact value of $m_\chi > 0.188 \text{ GeV}$ that marks the transition from two critical values to one critical value for f_χ must lie in the range $0.4 < m_\chi/\text{GeV} < 0.56$. For this particular value of m_χ , the largest root of the equation $M_{lim}(f_\chi, m_\chi) = 2 M_\odot$ is $f_\chi \approx 100\%$.

The critical DM fraction is shown in Fig. (7) by the heavy black curve labeled $f_\chi^{crit}(m_\chi)$. The green region in the same figure thus represents the portion of the (m_χ, f_χ) plane where the calculated maximum mass for DANS is compatible with the present measured masses of “heavy” neutron stars with $M_{tot} \sim 2 M_\odot$ [53, 54]. It is useful to observe that, in the range $10 \leq m_\chi/\text{GeV} \leq 100$ the critical DM curve $f_\chi^{crit}(m_\chi)$ is well described by the following equation

$$f_\chi^{crit}(m_\chi) = 31.15 \left(\frac{1 \text{ GeV}}{m_\chi} \right)^2 + 6.62 \times 10^{-6} \quad (7)$$

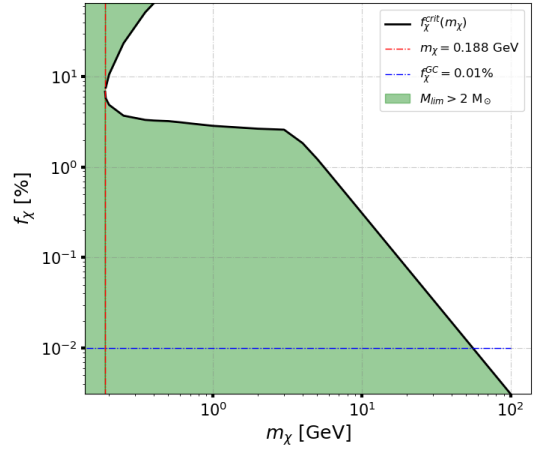


FIG. 7. Critical value of f_χ as a function of m_χ . In the green region and along the black line the maximum mass for DANS is compatible with observation.

B. Proton fraction and direct URCA processes in DANS

As we show in this subsection, the presence of DM influences not only the bulk properties (mass, radius, maximum mass) of a neutron star, but in addition has indirect sizeable effect (through gravitational interaction) on the particle fractions of the OM fluid constituents when considering DANS with a fixed total gravitational mass. In particular the value of f_χ influences the proton fraction $x_p = n_p/n$ (with $n = n_n + n_p$ being the baryon number density) in β -stable nuclear matter. As has been shown in Ref. [40], when the proton fraction x_p is larger than a threshold value, denoted as x_p^{durca} , the so-called direct URCA processes $n \rightarrow p + e^- + \bar{\nu}_e$, $p + e^- \rightarrow n + \nu_e$, can occur in neutron star matter. The direct URCA processes enhances neutrino emission and neutron star cooling rates by a very large factor compared to the so-called modified URCA processes $(n, p) + n \rightarrow p + e^- + \bar{\nu}_e$, $(n, p) + p + e^- \rightarrow n + \nu_e$, causing a fast cooling of the star [40, 41].

In β -stable nuclear matter the threshold proton fraction for direct URCA processes can be written [25]

$$x_p^{durca} = \frac{1}{1 + (1 + Y_e^{1/3})^3}, \quad (8)$$

where $Y_e = n_e/(n_e + n_\mu)$ is the leptonic electron fraction. Notice that below the muon threshold density $x_p^{durca} = 1/9$ while for asymptotically large baryon densities $x_p^{durca} \sim 14.77\%$.

In Fig. 8, we plot the proton fraction x_p in β -stable nuclear matter as a function of the radial coordinate r_{OM} in a DANS having a total gravitational mass $M_{tot} = 1.4 M_\odot$ and considering three different values, $f_\chi = 0\%$, 3.1% , 5.41% , for the DM fraction (continuous lines) and taking $m_\chi = 1 \text{ GeV}$. Each of the three dash-dotted lines represents the threshold proton fraction x_p^{durca} for

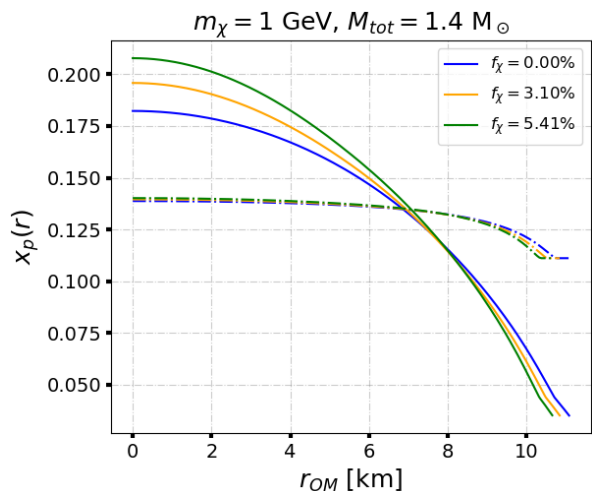


FIG. 8. Proton fraction $x_p(r)$ (continuous lines) and direct URCA processes threshold (dash-dotted lines) $x_p^{durca}(r)$ as functions of the radial coordinate in the ordinary matter fluid for a DANS having a gravitational mass $M_{tot} = 1.4 M_\odot$ in the case $m_\chi = 1$ GeV and different values of f_χ .

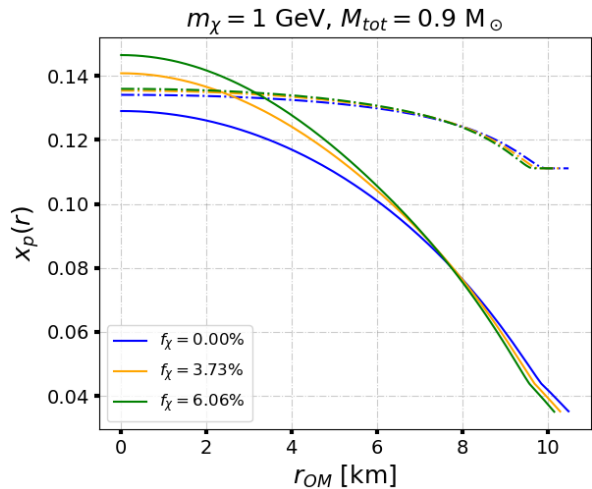


FIG. 9. Same as in Fig. 8 but now for $M_{tot} = 0.9 M_\odot$.

the direct URCA processes associated to the x_p curve with the same f_χ (curves with the same color). The intersection point between each couple of curves with the same color gives the value of the radial coordinate r_{OM}^{durca} below which direct URCA processes are possible. As is clearly seen in Fig. 8, the presence a DM core produces a significant increase in the proton fraction (particularly in the central region of the star) and small increase in the value of r_{OM}^{durca} . Notice that in the case of an ordinary neutron star ($f_\chi = 0$) with mass $M = 1.4 M_\odot$ described by the BL EOS, direct URCA processes are already possible [25]. Complementary to Fig. 8, we report in Tab. II some of the properties of a DANS with $M_{tot} = 1.4 M_\odot$ in the case $m_\chi = 1$ GeV.

Fig. 9 displays the same physical quantities as in the

f_χ [%]	$n(r=0)$ [fm^{-3}]	$x_p(r=0)$	r_{OM}^{durca} [km]
0	0.497	0.182	6.84
3.10	0.539	0.196	6.94
5.41	0.578	0.208	7.08

TABLE II. Central baryon number density (second column), central proton fraction (third column) and the radial coordinate r_{OM}^{durca} below which direct URCA processes are possible in a $1.4 M_\odot$ DANS for different value of the dark matter fraction f_χ (first column). All the results are relative to the case $m_\chi = 1$ GeV.

f_χ [%]	$n(r=0)$ [fm^{-3}]	$x_p(r=0)$	r_{OM}^{durca} [km]
0	0.345	0.129	/
3.73	0.377	0.141	2.40
6.06	0.393	0.147	3.13

TABLE III. Same as Tab. II but for $M_{tot} = 0.9 M_\odot$.

previous figure, but this time for DANS with a total gravitational mass $M_{tot} = 0.9 M_\odot$. Now in the case of ordinary neutron stars direct URCA processes are not possible ($x_p < x_p^{durca}$), but they can be switched on if a sufficient amount of DM is present in the star. Complementary to Fig. 9, we report in Tab. III some of the properties of a DANS with $M_{tot} = 0.9 M_\odot$ in the case $m_\chi = 1$ GeV.

The calculated values for the threshold baryon number density n^{durca} for having direct URCA processes and the corresponding threshold proton fraction $x_p(n^{durca})$ do not depend on the DM fraction, since these two quantities are exclusively determined by the nuclear interactions and particularly are strongly affected by the density dependence of the nuclear symmetry energy [37]. In the case of the BL EOS one has $n^{durca} = 0.361 \text{ fm}^{-3}$ and $x_p(n^{durca}) = 0.1347$ [25]. The stellar total gravitational mass $M_{tot}^{durca} \equiv M_{tot}(n_c = n^{durca})$ beyond which direct URCA processes are possible depends instead on the DM fraction. Its value together with the value of the gravitational maximum mass M_{tot}^{max} is reported in Tab. IV for some values of the DM fraction. As we see the presence of a DM core reduces the value of M_{tot}^{durca} and thus makes possible fast cooling of "light" neutron stars.

f_χ [%]	M_{tot}^{durca} [M_\odot]	M_{max} [M_\odot]
0	0.96	2.07
3.10	0.87	1.99
5.41	0.82	1.94

TABLE IV. Values for $M_{tot}^{durca} = M_{tot}(n^{durca})$ (second column) and for the maximum gravitational mass M_{max} for DANS sequences for different values of dark matter fraction (first column). The third column reports values of obtained for the corresponding f_χ value. All the results are relative to the case $m_\chi = 1$ GeV.

V. CONSTRAINTS FROM ASTROPHYSICAL OBSERVATIONS ON DM PROPERTIES

As discussed in [19], it is possible to give an upper limit to the dark matter particles mass by using the results obtained in figure (7) and comparing them with an estimation of the amount of dark matter that can be accumulated onto a neutron star. Such an estimation requires to evaluate the dark matter accretion rate at every evolutionary stage of the star, from the formation of the progenitor star to the stable neutron star stage. Dark matter accretion rate onto neutron stars as been discussed in [58] and the total amount of dark matter accumulated in a given time t can be written as (see [19])

$$M_{DM}^{acc} \approx 10^{-14} \left(\frac{\rho_\chi}{0.3 \text{ GeV/cm}^3} \right) \left(\frac{\sigma_{\chi n}}{10^{-45} \text{ cm}^2} \right) \left(\frac{t}{1 \text{ Gyr}} \right) M_\odot \quad (9)$$

where ρ_χ is the local dark matter density and $\sigma_{\chi n}$ is the dark matter-nucleon interaction cross section.

Following [19], by using the Einasto profile for ρ_χ [59–62], assuming $\sigma_{\chi n} \sim 10^{-45} \text{ cm}^2$ and $t \sim 10 \text{ Gyr}$, we can estimate $M_{DM}^{acc} \sim (10^{-14} - 10^{-13}) M_\odot$ for a $2 M_\odot$ mass neutron star in the disk of our galaxy. This values are too low to put a stringent upper limit on m_χ . As discussed in [19], using equation (9), for a $2 M_\odot$ mass neutron stars in the central region of our galaxy, we find that $f_\chi \leq 0.01\%$. Using this estimation, equation (7) give us an upper limit for the dark matter particles:

$$m_\chi \leq 56 \text{ GeV} \quad (10)$$

which is close to the result obtained in [19] ($m_\chi \leq 60 \text{ GeV}$) in spite the fact that we are using a different EOS for ordinary matter.

We observe that in the dark matter accretion rate estimation made in [58], only the dark matter-nucleon interaction cross-section is taken into account. If we assume a non zero self interaction between dark matter particles, the accretion rate and the result in equation (10) may change drastically.

VI. STABILITY OF DANS

A solution the two-fluid TOV equations (1) and (2) represents an equilibrium configuration. In this section we present results regarding the stability with respect to small radial perturbation of DANS. We assume that these perturbations don't modify the β -equilibrium condition of ordinary matter.

In the one-fluid limit (stars made only of ordinary matter or only of dark matter) it is well known that the critical point is the maximum of the $M(\rho_{c,j})$ curve [52]. Using the EOSs considered in this work we get the following value for the central mass densities of the critical config-

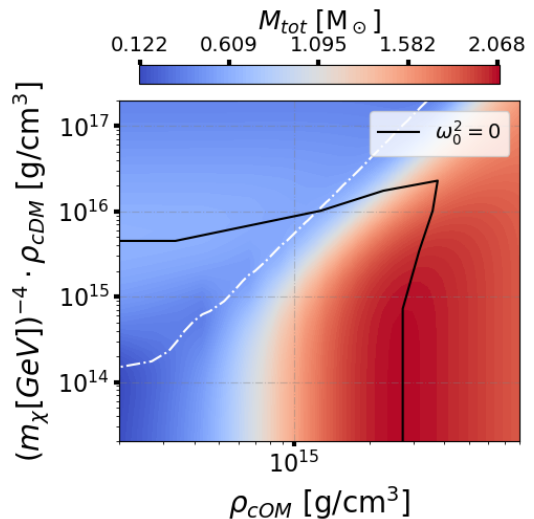


FIG. 10. Critical stability curve for $m_\chi = 1 \text{ GeV}$. The white dashed line is the $\Delta R = R_{OM} - R_{DM} = 0$ contour line.

uration

$$\text{OM stars: } \rho_{cOM} = 2.727 \times 10^{15} \text{ g/cm}^3$$

$$\text{DM stars: } \rho_{cDM} = 5.362 \times 10^{15} \left(\frac{m_\chi}{1 \text{ GeV}} \right)^4 \text{ g/cm}^3$$

In the two-fluids system case we get a critical stability curve in the (ρ_{cOM}, ρ_{cDM}) plane.

The stability analysis can be done in two different ways. The first method, discussed by Kain in [21], requires to solve a set of pulsation equations whose solution give the squared radial oscillation frequency ω^2 . If the squared radial oscillation frequency for the fundamental mode ω_0^2 is positive, than the corresponding solution is stable while, if $\omega_0^2 < 0$, the solution is unstable. This method requires to take the derivative of the EOSs of the fluids which is a problem if the EOSs aren't smooth enough.

The second method, developed by Henriques, Liddle and Moorhouse in [63], allow us to determine the critical stability curve without solving the pulsation equations. Their analysis give the following equation for the critical stability curve

$$\frac{dM_{tot}}{d\vec{\sigma}} = \frac{dN_{OM}}{d\vec{\sigma}} = \frac{dN_{DM}}{d\vec{\sigma}} = 0 \quad (11)$$

where M_{tot} , N_i ($i = OM, DM$) are the total gravitational mass and total fluid number of a static solution and $\vec{\sigma}$ is a vector in the parameter space that is simultaneously tangent to the level curves of M_{tot} and N_i . It can be shown [63] that if two of the quantities in (11) are zero, then the third is also zero so, to determine the critical stability curve, we can study the stationary point of M_{tot} along level curve of N_{DM} . As observed in [63], the stability region in the (ρ_{cOM}, ρ_{cDM}) plane must contain the stable structure in the one-fluid limit.

Figure (10) shows results obtained for $m_\chi = 1 \text{ GeV}$. This results are similar to those obtained by Kain in [22] and

show us that we can have stable DANS with both a core and a dark matter halo. We also note that there is a region inside the stability curve where DANS have an ordinary matter central density and/or a dark matter central density that exceed the critical value in the one-fluid limit.

VII. SUMMARY

In this paper we have studied the consequences of the presence of DM on the structural properties and the stability of neutron stars. Specifically, we explored how the properties of these DANS are modified with respect to those of ordinary neutron stars in terms of the DM particle mass m_χ and the fraction of DM present in the star. To model ordinary matter we used a state-of-the-art equation of state of β -stable nuclear matter obtained using the Brueckner-Hartree-Fock quantum many-body approach starting from two-body and three-body nuclear interactions derived from chiral effective field theory. This EOS, as discussed in Sect. III A, reproduces various empirical nuclear matter properties at the satu-

ration density n_0 and at supranuclear densities ($n > n_0$). Additionally, the calculated $E_{sym}(n_0)$ and L fulfill the bounds imposed by the unitary Fermi gas limit [29]. The dark matter component of the star has been modeled as a non-self-annihilating system of spin 1/2 fermions and its EOS as an ideal relativistic Fermi gas. We found that, depending on the dark matter particle mass m_χ , one can have somehow opposite effects on the stellar properties. In fact, in the case $m_\chi = 1$ GeV, the stellar gravitational maximum mass M_{max} decreases, whereas in the case $m_\chi = 0.1$ GeV M_{max} increases with respect to the maximum mass of ordinary neutron stars. We studied M_{max} as a function of f_χ for some values of m_χ . Following [19], we defined the critical values $f_\chi^{crit}(m_\chi)$ as the roots of the equation $M(f_\chi, m_\chi) = 2 M_\odot$ for a given value of m_χ . Comparing an upper limit for the total dark matter fraction accumulated by a $2 M_\odot$ neutron star in the galactic center with the function $f_\chi^{crit}(m_\chi)$, we found an upper limit for the dark matter particles: $m_\chi \leq 56$ GeV. We also shown that the presence of dark matter has indirect sizeable effect on the proton fraction in the ordinary matter fluid and, in the case $m_\chi = 1$ GeV, results in a decrease of the threshold gravitational mass M_{tot}^{durca} for having direct URCA processes and fast stellar cooling.

-
- [1] E. Corbelli and P. Salucci, Monthly Notices of the Royal Astronomical Society **311**, 441 (2000).
 - [2] F. Nesti, P. Salucci, and N. Turini, Astronomy **2**, 90 (2023).
 - [3] P. J. E. Peebles, The Astrophysical Journal Letters **263**, L1 (1982).
 - [4] G. Goldhaber and S. Perlmutter, Physics Reports **307**, 325 (1998).
 - [5] P. M. Garnavich, R. P. Kirshner, P. Challis, J. Tonry, R. L. Gilliland, R. C. Smith, A. Clocchiatti, A. Diercks, A. V. Filippenko, M. Hamuy, C. J. Hogan, B. Leibundgut, M. M. Phillips, D. Reiss, A. G. Riess, B. P. Schmidt, R. A. Schommer, J. Spyromilio, C. Stubbs, N. B. Suntzeff, and L. Wells, Astrophysical Journal **493**, L53 (1998).
 - [6] Y. Sofue, Publications of the Astronomical Society of Japan **65**, 118 (2013).
 - [7] M. Pato, F. Iocco, and G. Bertone, Journal of Cosmology and Astroparticle Physics **2015**, 001 (2015).
 - [8] H.-N. Lin and X. Li, Monthly Notices of the Royal Astronomical Society **487**, 5679 (2019).
 - [9] E. Aprile, J. Aalbers, F. Agostini, M. Alfonsi, F. Amaro, M. Anthony, F. Arneodo, P. Barrow, L. Baudis, B. Bauermeister, et al., Physical Review Letters **119**, 181301 (2017).
 - [10] G. Bertone and M. Fairbairn, Physical Review D **77**, 043515 (2008).
 - [11] A. de Lavallaz and M. Fairbairn, Physical Review D **81**, 123521 (2010).
 - [12] C. Kouvaris and P. Tinyakov, Physical Review D **82**, 063531 (2010).
 - [13] C. Kouvaris and P. Tinyakov, Physical Review D **83**, 083512 (2011).
 - [14] S.-C. Leung, M.-C. Chu, and L.-M. Lin, Physical Review D **84**, 107301 (2011).
 - [15] P. Ciarcelluti and F. Sandin, Physics Letters B **695**, 19 (2011), arXiv:1005.0857 [astro-ph.HE].
 - [16] C. Kouvaris et al., Advances in High Energy Physics **2013** (2013).
 - [17] C. Kouvaris and N. G. Nielsen, Physical Review D **92**, 063526 (2015).
 - [18] J. Ellis, G. Hütsi, K. Kannike, L. Marzola, M. Raidal, and V. Vaskonen, Physical Review D **97**, 123007 (2018).
 - [19] O. Ivanytskyi, V. Sagun, and I. Lopes, Physical Review D **102**, 063028 (2020).
 - [20] A. Del Popolo, M. Deliyergiyev, M. Le Delliou, L. Tolos, and F. Burgio, Physics of the Dark Universe **28**, 100484 (2020).
 - [21] B. Kain, Physical Review D **102**, 023001 (2020).
 - [22] B. Kain, Physical Review D **103**, 043009 (2021).
 - [23] S. Shakeri and D. R. Karkevandi, Phys. Rev. D **109**, 043029 (2024), arXiv:2210.17308 [astro-ph.HE].
 - [24] G. Bertone, D. Hooper, and J. Silk, Physics Reports **405**, 279 (2005).
 - [25] I. Bombaci and D. Logoteta, Astron. Astrophys. **609**, A128 (2018), arXiv:1805.11846 [astro-ph.HE].
 - [26] R. Machleidt and D. R. Entem, Phys. Rept. **503**, 1 (2011), arXiv:1105.2919 [nucl-th].
 - [27] H. W. Hammer, S. König, and U. van Kolck, Reviews of Modern Physics **92**, 025004 (2020).
 - [28] D. Logoteta, I. Bombaci, and A. Kievsky, Phys. Rev. C **94**, 064001 (2016), arXiv:1609.00649 [nucl-th].
 - [29] I. Tews, J. M. Lattimer, A. Ohnishi, and E. E. Kolomeitsev, Astrophysical Journal **848**, 105 (2017), arXiv:1611.07133 [nucl-th].

- [30] A. Kievsky, M. Viviani, D. Logoteta, I. Bombaci, and L. Girlanda, *Physical Review Letters* **121**, 072701 (2018), arXiv:1806.02636 [nucl-th].
- [31] P. Danielewicz, R. Lacey, and W. G. Lynch, *Science* **298**, 1592 (2002), arXiv:nucl-th/0208016.
- [32] P. Danielewicz and J. Lee, *Nuclear Physics A* **922**, 1 (2014).
- [33] X. Roca-Maza, M. Brenna, B. K. Agrawal, P. F. Bortignon, G. Colò, L.-G. Cao, N. Paar, and D. Vretenar, *Phys. Rev. C* **87**, 034301 (2013), arXiv:1212.4377 [nucl-th].
- [34] I. Bombaci and U. Lombardo, *Phys. Rev. C* **44**, 1892 (1991).
- [35] B.-A. Li, B.-J. Cai, W.-J. Xie, and N.-B. Zhang, *Universe* **7** (2021), 10.3390/universe7060182.
- [36] N.-B. Zhang and B.-A. Li, *The Astrophysical Journal* **921**, 111 (2021).
- [37] I. Bombaci, in *Astrophysics and Space Science Library*, *Astrophysics and Space Science Library*, Vol. 465, edited by S. Bhattacharyya, A. Papitto, and D. Bhattacharya (2022) pp. 281–317.
- [38] J. M. Lattimer and M. Prakash, *Astrophys. J.* **550**, 426 (2001), arXiv:astro-ph/0002232 [astro-ph].
- [39] A. W. Steiner, *Phys. Rev. C* **74**, 045808 (2006), arXiv:nucl-th/0607040 [nucl-th].
- [40] J. M. Lattimer, C. J. Pethick, M. Prakash, and P. Haensel, *Phys. Rev. Lett.* **66**, 2701 (1991).
- [41] D. Page, J. M. Lattimer, M. Prakash, and A. W. Steiner, *The Astrophysical Journal Supplement Series* **155**, 623 (2004), arXiv:astro-ph/0403657 [astro-ph].
- [42] D. Logoteta and I. Bombaci, *Universe* **5**, 204 (2019).
- [43] B. P. Abbott et al. (LIGO Scientific, Virgo), *Phys. Rev. Lett.* **119**, 161101 (2017), arXiv:1710.05832 [gr-qc].
- [44] D. Logoteta, A. Perego, and I. Bombaci, *Astron. Astrophys.* **646**, A55 (2021), arXiv:2012.03599 [nucl-th].
- [45] S. Bernuzzi et al., *Mon. Not. Roy. Astron. Soc.* **497**, 1488 (2020), arXiv:2003.06015 [astro-ph.HE].
- [46] A. Endrizzi, D. Logoteta, B. Giacomazzo, I. Bombaci, W. Kastaun, and R. Ciolfi, *Phys. Rev. D* **98**, 043015 (2018), arXiv:1806.09832 [astro-ph.HE].
- [47] A. Prakash, D. Radice, D. Logoteta, A. Perego, V. Nedora, I. Bombaci, R. Kashyap, S. Bernuzzi, and A. Endrizzi, *PHYSICAL REVIEW D* **104** (2021), 10.1103/PhysRevD.104.083029.
- [48] G. Baym, C. Pethick, and P. Sutherland, *Astrophys. J.* **170**, 299 (1971).
- [49] J. W. Negele and D. Vautherin, *Nucl. Phys. A* **207**, 298 (1973).
- [50] D. E. Kaplan, M. A. Luty, and K. M. Zurek, *Phys. Rev. D* **79**, 115016 (2009), arXiv:0901.4117 [hep-ph].
- [51] K. M. Zurek, *Phys. Rep.* **537**, 91 (2014), arXiv:1308.0338 [hep-ph].
- [52] S. L. Shapiro and S. A. Teukolsky, *Black holes, white dwarfs and neutron stars. The physics of compact* (1983).
- [53] J. Antoniadis, P. C. C. Freire, N. Wex, T. M. Tauris, R. S. Lynch, M. H. van Kerkwijk, M. Kramer, C. Bassa, V. S. Dhillon, T. Driebe, J. W. T. Hessels, V. M. Kaspi, V. I. Kondratiev, N. Langer, T. R. Marsh, M. A. McLaughlin, T. T. Pennucci, S. M. Ransom, I. H. Stairs, J. van Leeuwen, J. P. W. Verbiest, and D. G. Whelan, *Science* **340**, 448 (2013), arXiv:1304.6875 [astro-ph.HE].
- [54] E. Fonseca et al., *Astrophys. J. Lett.* **915**, L12 (2021), arXiv:2104.00880 [astro-ph.HE].
- [55] M. Miller, F. K. Lamb, A. Dittmann, S. Bogdanov, Z. Arzoumanian, K. C. Gendreau, S. Guillot, A. Harding, W. Ho, J. Lattimer, et al., *The Astrophysical Journal Letters* **887**, L24 (2019).
- [56] B. P. Abbott et al. (The LIGO Scientific Collaboration and the Virgo Collaboration), *Phys. Rev. Lett.* **121**, 161101 (2018).
- [57] V. Sagun, V. Sagun”, E. Giangrandi”, O. Ivanytskyi”, I. Lopes”, and K. Bugaev, in *Proceedings of Particles and Nuclei International Conference 2021* — (Sissa Medialab) p. 313.
- [58] C. Kouvaris, *Physical Review D* **77**, 023006 (2008).
- [59] J. Einasto, *Trudy Astrofizicheskogo Instituta Alma-Ata* **5**, 87 (1965).
- [60] J. Einasto, *Astrofizika* **5**, 137 (1969).
- [61] D. Merritt, A. W. Graham, B. Moore, J. Diemand, and B. Terzić, *Astronomical Journal* **132**, 2685 (2006), arXiv:astro-ph/0509417 [astro-ph].
- [62] M. Baes, *Astronomy & Astrophysics* **667**, A47 (2022), arXiv:2209.03639 [astro-ph.GA].
- [63] A. Henriques, A. R. Liddle, and R. Moorhouse, *Physics Letters B* **251**, 511 (1990).